Title
First-principles study on shape of intrinsic hBN island nucleated during CVD initial growth on Cu(111)

Author(s)
Imamura Ryo / KAGESHIMA Hiroyuki

Journal
Japanese Journal of Applied Physics 63 (4)

Published
2024-04-05

URL (The Version of Record)
https://doi.org/10.35848/1347-4065/ad2bbe

First-principles study on shape of intrinsic hBN island nucleated during CVD initial growth on Cu(111)

Ryo Imamura[1] and Hiroyuki Kageshima[1]*

[1]*Shimane University, 1060 Nishi-Kawatsucho Matsue 690-8504, Japan*

E-mail: n23m202@matsu.shimane-u.ac.jp

Abstract

Focusing on the edge of small monolayer hBN islands on Cu(111) and intrinsic nucleation during the CVD initial growth, the shape of hBN islands is investigated utilizing the first-principles calculation. Several key observations have been made. Firstly, it is ascertained that desorption does not play a decisive role in shaping the islands. Next, it is found that, for small islands, there is no chemical potential range where the armchair edge is stable. Then, it is identified that, the bonds between Cu atoms on the surface and N atoms at the edge are strong, while the bonds between Cu atoms on the surface and B atoms at the edge are comparatively weaker. Furthermore, it is found that triangular islands with N edge tend to grow more spontaneously than those with B edge because the critical size is smaller for those with N edge across a wide chemical potential range.

1. Introduction

The ultrathin two-dimensional semiconductor layered materials are promising as future materials for electronic devices, and hexagonal boron nitride (hBN) stands out as the most useful candidate for their insulating films. hBN is an atomically thin two-dimensional material where boron (B) and nitrogen (N) are arranged in a honeycomb pattern, having a band gap of 5.97 eV.[1, 2)] hBN is widely applied as an insulating film in transistors employing two-dimensional semiconductors, exhibiting a room temperature mobility of 40000 $cm^2 V^{-1} s^{-1}$ when combined with bilayer graphene.[3)] Moreover, combining it with molybdenum disulfide (MoS_2) significantly reduces traps induced by strain at the interface.[4)] These properties drastically attract hBN, enabling enhanced mobility and decreased interface-related degradation in electronic devices.

hBN is primarily produced using two methods: high-pressure and high-temperature (HP/HT) synthesis,[1, 2)] and chemical vapor deposition (CVD) growth.[10-22)] Much of the research on transistor applications utilizes hBN obtained through mechanical exfoliation from HP/HT synthesis,[3-9)] as the quality of mechanically exfoliated hBN to be superior to that grown through CVD. However, mechanically exfoliated hBN typically achieves only lateral sizes of several tens of micrometers.[4-6)] Conversely, CVD-grown hBN has achieved sizes up to several centimeters.[10)] Therefore, if the quality of CVD-grown hBN can be enhanced to match or surpass that of mechanically exfoliated hBN, the potential applications of hBN will broaden.

CVD growth utilizes borazine ($B_3N_3H_6$) or ammonia borane (BH_3-NH_3) as source materials along with various metals as substrate materials. For instance, in producing a multilayer structure, the iron-nickel (Fe-Ni) alloy serves as a suitable substrate since the dissolved B and N within the substrate will precipitate, allowing for easy control over thickness uniformity.[10-12)] Furthermore, in producing a monolayer structure, copper (Cu), cobalt (Co), or platinum (Pt) are suitable substrates as they exhibit minimal dissolution of B and N into the substrate.[13-22)]

We specifically investigate the CVD growth of hBN on Cu substrates. Previous reports indicate that monolayer hBN islands formed during CVD growth on metal substrates like Cu and Co are predominantly triangular shape.[13-15, 18, 20-22)] To produce high-quality hBN, it is crucial for these triangular islands to be uniformly oriented and for the number of islands formed to be minimal. When triangular islands are formed with varying orientations, they tend to become polycrystalline and exhibit lower quality. Enhancing quality requires a comprehensive understanding of the CVD growth mechanism, including the types of islands

formed and their formation process.

The previous theoretical study reported that the triangular shape of hBN on Cu(111) is either stable or unstable depending on the chemical potential of B.[23] However, this study made assumptions based on large hBN islands and exclusively focused on edge stability, neglecting cases where the hBN island is rather small as the very initial stage of crystal growth. In our current theoretical study, we specifically examine the edges of very small monolayer hBN islands, assuming intrinsic nucleation during the early stages of CVD growth. We investigate the correlation between the shape of hBN islands and the edge effect. This paper presents an expanded version of Ref. 24, incorporating additional data and discussions.

2. Computational methods

We performed the first-principles calculations based on the density functional theory (DFT) using PHASE/0.[25] All calculations were based on the projector augmented wave (PAW) method[26] and the PAW ultrasoft-pseudopotentials. The cutoff energy of the plane wave basis is set to 30 Ry, and we applied two types of van der Waals force corrections, namely rev-vdW-DF2 (B86r)[27] and GGA-PBE + D3 (D3).[28, 29] To model Cu(111), we used the 6×6 lateral supercell. The slab thickness consists of 3 Cu layers, and the superslab geometry includes a vacuum layer of 11 Å. Consequently, the unit cell dimensions are determined by lateral lattice constants of 15.37 Å each and a c-axis lattice constant of 15.19 Å. The unit cell angles of α, β, and γ are set to 120°, 90°, and 90°, respectively. We employed the Monkhorst-Pack method[30] for k-point sampling, and the number of k points was 2 × 2 × 1.

We performed the first-principles calculations by placing various hBN islands on Cu(111). In this configuration, B was positioned at the hollow site directly above the Cu atom in the third layer from the top, and N was positioned above the Cu atom (Figs. 1 and S1). This is based on the fact that this configuration was the most stable in our study with B86r using hexagonal hBN islands with 7 six-membered rings (Figs. S1 and S2). This trend is also confirmed to be the same in our study with D3, and is also consistent with other previous studies on hBN on metal surfaces.[21, 31-33] We calculated hBN islands with 1 to 10 six-membered rings, exploring various geometries such as B edge (Btri), N edge (Ntri), ribbon shape (BNrib), armchair (BNa), armchair with zigzag mixed edge (BNmix), and other structures. All atomic positions were optimized while keeping the Cu layer on the back side fixed in an ideal position.

Next, we compared and evaluated the stability of each calculated hBN island structure

using the formation energy (E_f). In this study, the formation energy is defined as

$$E_f = E_{tot} - E_{Cu} - n_B\mu_B - n_N\mu_N, \qquad (1)$$

where E_{tot} is the total energy of the system with the adsorbed hBN island, E_{Cu} the total energy of Cu substrate without hBN islands, n_B the number of B atoms constituting the hBN island, n_N the number of N atoms constituting the hBN island, μ_B the chemical potential of B, and μ_N the chemical potential of N.

In this study, the chemical potential is considered as a variable. hBN, being a binary material consisting of B and N, makes it impossible to determine the formation energy without defining the chemical potential μ_B and μ_N. Once the experimental conditions are established, μ_B and μ_N at that specific time and location should be determined if it is in macroscopic level. However, the chemical reactions involved in surface crystal growth are non-equilibrium, in microscopic level, and tremendously complex. As such, determining the exact values of μ_B and μ_N remains an unresolved problem, requiring in-depth study beyond the scope of this research, and is considered a future challenge.

Thus, a common approach in theoretical study is to consider μ_B and μ_N by considering various possibilities, including highly extreme possibilities. This approach provides a comprehensive overview of the potential for hBN growth across diverse environments and conditions, enhancing our understanding of the actual experimental crystal growth mechanisms.

Previous theoretical studies have followed a similar approach. In the early stages, this methodology was conceptualized and implemented in the theoretical study by Van de Walle, et al.[34] They calculated and discussed formation energies across a wide range of gallium (Ga) chemical potential μ_{Ga} and N chemical potential μ_N to investigate phase transitions in surface reconstruction on GaN surfaces. Since then, such an analytical approach they utilized has been widely adopted by numerous researchers. For instance, Yakobson's group investigates the edge energy and island shape of hBN islands, proposing that the edge energy determines the stability of free-standing hBN as well as hBN on Cu(111) and Ni(111).[23, 35] In these studies, chemical potentials μ_B and μ_N are also varied widely.

In addition, we have configured the chemical potential so that the sum of μ_B and μ_N is consistently conserved. As mentioned above, our aim is to investigate the outcomes when μ_B and μ_N are varied across a wide range. Nevertheless, treating μ_B and μ_N as entirely independent variables would lead to an expansive array of possibilities, making it exceedingly challenging to investigate comprehensively. Therefore, since hBN is growing, we approximated the sum of μ_B and μ_N to be the total energy of the flee-standing hBN

sheet per BN pair, so as to represent a case where the surface B and N are in close chemical equilibrium with the hBN sheet. Of course, this is not a necessary and sufficient condition, and deviations are possible. However, it might be reasonable enough to assume that the chemical potentials are within this framework. This conceptualization is also utilized by Yakobson's group in their previous studies.[23, 35] We acknowledge that a future work involves studying the deviations from these conditions and understanding their implications.

From the perspective of considering the various possibilities of μ_{B} and μ_{N}, we can consider the upper limit of μ_{B} as the chemical potential of α-boron (B_{50}), a solid composed entirely of B. Similarly, the upper limit of μ_{N} can be considered as the chemical potential of the nitrogen molecule (N_2). Therefore, we have defined B-rich and N-rich as the limits of both, as described below. μ_{B} and μ_{N} can take any value between the upper and lower limits, but since it is not practical to give examples of all possible values, we will frequently use the terms B-rich and N-rich in the following sections. Once these limits are known, it might be easy to imagine what happens at any intermediate chemical potential.

After all, in this study, we configured such that $\mu_{\mathrm{B}} + \mu_{\mathrm{N}} = E_{\mathrm{hBN}}$, where E_{hBN} is the total energy per BN pair of the free-standing hBN sheet. The calculated values are −541.0 eV with B86r and −541.8 eV with D3. μ_{B} and μ_{N} are derived as follows:

$$\mu_{\mathrm{B}}^{0} = \frac{E_{\mathrm{B_{50}}}}{50}, \qquad (2)$$

$$\mu_{\mathrm{N}}^{0} = E_{\mathrm{hBN}} - \mu_{\mathrm{B}}^{0}, \qquad (3)$$

$$\mu_{\mathrm{B}}^{1} = E_{\mathrm{hBN}} - \mu_{\mathrm{N}}^{1}, \qquad (4)$$

$$\mu_{\mathrm{N}}^{1} = \frac{E_{\mathrm{N_2}}}{2}, \qquad (5)$$

where the labels 0 and 1 represent B-rich and N-rich, respectively. μ_{B}^{0}, μ_{N}^{0}, μ_{B}^{1}, and μ_{N}^{1} are μ_{B} in the B-rich, μ_{N} in the B-rich, μ_{B} in the N-rich, and μ_{N} in the N-rich, respectively. $E_{\mathrm{B_{50}}}$ and $E_{\mathrm{N_2}}$ are the total energies of B_{50} and N_2, respectively. We will discuss the formation energies in the both extreme conditions, B-rich and N-rich.

Finally, we evaluated the energies of the edge and non-edge parts of the hBN islands. The atoms composing the hBN islands can be categorized into three groups: B atoms at the edge (edge B), N atoms at the edge (edge N), and the remaining atoms (inside atoms) [Fig. 1 (d)]. The energies of each atom are denoted as ε_{B}, ε_{N}, and $\varepsilon_{\mathrm{in}}$, respectively. In this study, we assumed that the formation energy can be calculated by

$$E_{\mathrm{f}} = i_{\mathrm{B}}\varepsilon_{\mathrm{B}} + i_{\mathrm{N}}\varepsilon_{\mathrm{N}} + i_{\mathrm{in}}\varepsilon_{\mathrm{in}}, \qquad (6)$$

where i_{B}, i_{N}, and i_{in} are the number of edge B atoms, edge N atoms, and inside atoms, respectively. We formulated equations for Btri and Ntri when the number of six-membered

rings is 3, and for all islands when the number of six-membered rings is 6. Subsequently, we calculated ε_B, ε_N, and ε_{in} using these equations. At that time, we choose the equations for Btri and Ntri when the number of six-membered rings is 3, and swapped the one remaining equation, which requires to obtain the fixed values. Due to the existence of multiple combinations of equations, we calculated the average values of ε_B, ε_N, and ε_{in}. Then, using these average values, we estimated the formation energies by Eq. (6) and compared them to the raw data to discuss the edge effect of hBN islands on Cu(111).

3. Results and discussion

3.1 Most stable shapes for each size of hBN island

First, we calculated the formation energy in both N-rich and B-rich for hBN islands with 3 six-membered rings, and examined the chemical potential dependence of the stable structure [Fig. 2 (a)]. Here, the calculated values for μ_B^0, μ_N^0, μ_B^1, and μ_N^1 with B86r are -155.7 eV, -385.3 eV, -158.4 eV, and -382.6 eV, respectively. Additionally, the calculated values with D3 are -155.8 eV, -386.0 eV, -158.4 eV, and -383.4 eV, respectively. In the subsequent discussion, we use the normalized chemical potential $\bar{\mu}_N$, defined as

$$\bar{\mu}_N = \frac{\mu_N - \mu_N^0}{\mu_N^1 - \mu_N^0}, \qquad (7)$$

where $\bar{\mu}_N = 0$ corresponds to μ_N^0, B-rich, and $\bar{\mu}_N = 1$ corresponds to μ_N^1, N-rich. The labels Btri, Ntri, BNrib, and BNa in Fig. 2 (a) correspond to the structures shown in Fig. 1 (a), respectively.

Figure 2 (a) is shown in the formation energy plotted for each shape as a function of $\bar{\mu}_N$. In the range where $\bar{\mu}_N$ is smaller than 0.22 with B86r and 0.15 with D3, Btri is the most stable. Conversely, in the other range, Ntri is the most stable. BNrib and BNa are not the most stable at any $\bar{\mu}_N$. Thus, the most stable structures are Btri and Ntri, with Ntri exhibiting the widest stable range.

Next, we performed the similar calculations and analyzed for cases where the number of six-membered rings is 6 and 10. The chemical potential dependence of their the most stable structures is shown in Fig. 2 (b) and Fig. 2 (c), respectively. The labels Btri, Ntri, BNrib, BNa, and BNmix in Fig. 2 (b) correspond to the structures shown in Fig. 1 (b), and the other five labels (ex1-ex5) to the structures shown in Fig. S5. Furthermore, the labels Btri, Ntri, BNrib, and BNa in Fig. 2 (c) correspond to the structures shown in Fig. 1 (c), and the other eight labels (ex1-ex8) to the structures shown in Fig S7. In the calculations, structural optimization occasionally transformed islands into connected patches, partially expanding

to the whole unit cell. Additionally, there were a few islands that changed into structures with five-membered rings. We exclude these structures from the following discussions.

For hBN islands with 6 six-membered rings, BNmix is the most stable when $\bar{\mu}_N$ ranges from 0.20 to 0.39 with B86r and from 0.16 to 0.42 with D3. BNmix is the most stable, while the difference in formation energy between BNmix and BNrib is quite small, 0.09 eV with B86r and 0.08 eV with D3. Btri is the most stable in the range when $\bar{\mu}_N$ is smaller than 0.20 with B86r and 0.16 with D3. Furthermore, Ntri is the most stable when $\bar{\mu}_N$ is larger than 0.39 with B86r and 0.42 with D3. When the number of six-membered rings is 3, BNa is more stable than BNrib, but as the number of six-membered rings increases to 6, BNa becomes rather unstable. Thus, the most stable structures are Btri, BNmix, and Ntri. Additionally, Ntri has the widest stable range, as observed in the case of 3 six-membered rings.

Next, for hBN islands with 10 six-membered rings, BNrib is the most stable when $\bar{\mu}_N$ ranges from 0.05 to 0.64 with B86r and from 0.04 to 0.59 with D3. BNrib is the most stable, while the difference in formation energy between BNrib and ex3 (Fig. S7) is quite small, 0.11 eV with B86r and 0.18 eV with D3. Btri is the most stable when $\bar{\mu}_N$ is smaller than 0.05 with B86r and 0.04 with D3. Furthermore, Ntri is the most stable when $\bar{\mu}_N$ is larger than 0.64 with B86r and 0.59 with D3. As expected, BNa is unstable. Thus, the most stable structures are Btri, BNrib, and Ntri. Additionally, BNrib has the widest stable range.

These results indicate that triangular structures are not necessarily the only ones that remain stable, as hBN islands grow up to expand; hexagonal and ribbon-like shapes also become stable.

Figure 3 summarizes the chemical potential dependence of the most stable structures when the number of six-membered rings is 3, 6, and 10. In all cases, the most stable range is wider for Ntri than for Btri. For hBN island with 3 six-membered rings, only triangular structures are the most stable. However, as the islands grow up to expand, the most stable range of non-triangular structures, such as BNmix and BNrib, extends more widely around $\bar{\mu}_N = 0.5$. There is no significant difference between the calculation results with B86r and D3, but the most stable range of Btri is narrower for D3.

3.2 Free-standing hBN islands

To examine the effect between the edges of hBN islands and chemically bonded Cu, we performed calculations on hBN islands in the absence of Cu, referred to as free-standing hBN islands. Generally, we can obtain triangular structures after structural optimization.

However, in some cases, ribbon-shaped and some zigzag structures either collapsed into a mono ring, or formed ten-membered rings [Fig 4 (a)], or changed their shapes into ridiculously different ones from the original.

Therefore, we decided not to perform structural optimization. This decision means that only Cu was removed from the calculated hBN islands on Cu(111). Subsequently, we calculated the energy for only the hBN geometry without structural optimization and compared these results with those for hBN islands on Cu surface. This approach allows us to examine the effects of the chemical bond between the edge of the hBN island and the Cu surface, as well as the van der Waals force of inside atoms. We performed this calculation and analysis for hBN islands with 3, 6, and 10 six-membered rings and summarized the chemical potential dependence of the most stable structures in Fig. 4 (b).

First, in the case of 3 six-membered rings, only Ntri is the most stable. Next, in the case of 6 six-membered rings, BNmix is the most stable when $\bar{\mu}_{\mathrm{N}}$ is smaller than 0.70 with B86r and D3. Conversely, in this case, Ntri is the most stable in the other range. Thus, the most stable structures for 6 six-membered rings are BNmix and Ntri, with BNmix exhibiting the most stable in the widest range. Finally, in the case of 10 six-membered rings, ex3 [Fig 4 (c)] is the most stable when $\bar{\mu}_{\mathrm{N}}$ is smaller than 0.86 with B86r and D3. Conversely, in this case, Ntri is the most stable in the other range. Thus, the most stable structures for 10 six-membered rings are ex3 and Ntri, with ex3 exhibiting the most stable in the widest range. Notably, Btri is never within the most stable range in any cases.

These contrast with the case involving the Cu substrate in the following aspects: In the case of 6 six-membered rings, the most stable range of BNmix widens. In the case of 10 six-membered rings, ex3 is the most stable. And, Btri is not the most stable in any cases. These results suggest that the N edge stability regardless of the presence of Cu. On the other hand, the effect of chemical bonding with Cu significantly impacts the stability of the B edge. However, the stability of BNmix and ex3 cannot be explained by the same logic. This is because perhaps the armchair-like edge has something to do with their stability.

According to previous theoretical report, the most stable edge of the macro-sized free-standing hBN is sequentially zigzag B, armchair, and zigzag N.[35)] The most stable range of the armchair edge depends on the chemical potential. It is therefore not surprising that the stability of the armchair edge may has something to do. However, the instability of Btri in our results contradicts the previous report, which indicated that zigzag B edge is stable. Such inconsistency is probably caused by the tremendously small size or the curled shape of the

islands we are calculating. In fact, the hBN islands we calculated are not ideally flat on the Cu surface; they are curled, causing the center of the island to lift. Therefore, the curl of the hBN islands may be related to their stability. The discussion on the curl of hBN islands is provided in subsection 3.6.

We also examined the desorption energy based on the calculation results for free-standing hBN islands. The desorption energy (E_{de}) in our calculation was defined as $E_{\mathrm{de}} = -(E_{\mathrm{tot}} - E_{\mathrm{Cu}} - E_{\mathrm{fs}})$, where E_{fs} is the total energy of the optimized structure of free-standing hBN. The larger E_{de} indicates the significant difficulty in desorbing from the Cu surface. The probability of desorption (P) is then calculated using the Boltzmann factor: $P = \exp(-\frac{E_{\mathrm{de}}}{k_{\mathrm{B}}T})$, where k_{B} is the Boltzmann constant, and T the absolute temperature. Assuming condition for the CVD growth, T can be set to 1300 K. Here, P approaches 0 as E_{de} becomes large. Because all the desorption energies we calculated exceed 1 eV, P is quite small; $P = 1 \times 10^{-4}$ or less. Therefore, hBN islands during the CVD growth are difficult to desorb regardless of their shape. This means that hBN islands with 3 or more six-membered rings are rarely detached during the CVD growth. Therefore, desorption is not a determining factor in island shape during the CVD growth. However, the effect of hydrogen (H), which is always present during CVD growth, was not taken into account at all in this study. It will be a subject for future work.

3.3 Relationship between size of hBN island and formation energy

We also investigated how the formation energy changes as hBN islands expand. As shown in Fig. 5, we summarized the formation energy per atom for all calculated structures concerning hBN island sizes (n_{B} or n_{N}) in both B-rich and N-rich conditions. Fig. 5 (a) shows the case of formation energy in the B-rich as the function of n_{B}, (b) the case of formation energy in the B-rich as the function of n_{N}, (c) the case of formation energy in the N-rich as the function of n_{B}, and (d) the case of formation energy in the N-rich as the function of n_{N}. Additionally, the most stable structures for each n_{B} of Fig. 5 (a) is shown in Fig. S8, those for each n_{N} of Fig. 5 (b) in Fig. S9, those for each n_{B} of Fig 5 (c) in Fig. S10, and those for each n_{N} of Fig. 5 (d) in Fig. S11. Focusing on the most stable formation energies for each n_{B} (n_{N}) in Fig. 5, they are almost decrease functions in all cases. However, each graph has its own unique characteristics.

In Fig. 5 (a), structures with more edge B than edge N tend to be the most stable. Although the decreasing trend is gradual, this is thought to be due to the small energy difference

between edge B and edge N in the B-rich. Additionally, the most structures tend to be close to Btri. Therefore, a larger Btri is thought to be formed when the growth proceeds.

Similarly, Fig. 5 (b), also in the B-rich, exhibits the same decreasing trend in formation energy and the tendency for structures closer to Btri to be more stable. However, because our calculations are constrained to structures with 1-10 six-membered rings, the decreasing trend is unavoidably not monotonous at all; for example, an increase was observed for $n_{\mathrm{N}} = 7$.

Figure 5 (c) for the N-rich case is not monotonically decreasing, unlike Fig. 5 (a) for the B-rich case. At $n_{\mathrm{B}} = 7$, 11, 16, 17, and 18, it is an increasing function. Also, instead of Btri, Ntri is stable and appears to grow into Ntri. These differences are thought to be due to the rather large energy difference between edge B and edge N in the N-rich. Finally, for Fig. 5 (d) in the N-rich case, the difference from Fig. 5 (b) in the B-rich case is almost the same as the difference between Figs. 5 (c) and (a).

These results indicate that there are differences in the structure between B-rich and N-rich. In the B-rich case, the energy difference between edge B and edge N is small, while in the N-rich case, edge N is considerably more stable than edge B, as indicated by the decreasing trend in formation energy. This finding aligns with the Fig. 6, as we will discuss later. This suggests that edge N is more stable over a wide range of chemical potentials. Additionally, structures closer to Btri tended to be the most stable in the B-rich, while conversely, structures closer to Ntri tended to be the most stable in the N-rich. There are consistent with the calculated formation energies of hBN islands with 3, 6, and 10 six-membered rings.

By the way, we would like to consider the large-size limit in Fig. 5. We calculated the formation energy when Cu(111) is entirely covered by hBN, and obtained −0.06 eV/atom with B86r and −0.11 eV/atom with D3. Since this geometry lacks edges, the value of this formation energy is only determined by the van der Waals force between the inside atoms and the Cu surface. In principle, the formation energy per atom approaches this value as n_{B} or n_{N} increases. However, as shown in Fig. 5, the energy difference remains substantial for an island with n_{B} or $n_{\mathrm{N}} = 18$. This suggests that the edge has a significant effect on formation energy. Perhaps there exists a size of hBN island at which the influence of inside atoms surpasses the effect of edges concerning formation energy. To comprehend the shape of a macro-sized island, it is crucial to examine the effects of both edges and inside atoms on formation energy.

3.4 Evaluation of edge energy and inside energy

We calculated the edge energies ε_{B}, ε_{N} and $\varepsilon_{\mathrm{in}}$ using the method described in Section 2. The average values of ε_{B}, ε_{N}, and $\varepsilon_{\mathrm{in}}$ in the B-rich are 1.02 eV, 1.41 eV, and −0.02 eV, respectively, with B86r, and 1.04 eV, 1.32 eV, and −0.05 eV respectively, with D3. On the other hand, in the N-rich, they are 1.91 eV, 0.52 eV, and −0.01 eV, respectively, with B86r, and 1.89 eV, 0.47 eV, and −0.06 eV, respectively, with D3. In the B-rich case, ε_{B} is more stable, and ε_{N} is less stable, and vice versa in the N-rich case. However, the difference between ε_{B} and ε_{N} in the B-rich is 0.28 eV with B86r and 0.39 eV with D3, while in the N-rich, it is 1.39 eV with B86r and 1.42 eV with D3, suggesting that the N edge is more stable than the B edge. In our calculations, the edge energies are dominant and $\varepsilon_{\mathrm{in}}$ is small. However, $\varepsilon_{\mathrm{in}}$ does not vary significantly between N-rich and B-rich but differs between B86r and D3. Furthermore, $\varepsilon_{\mathrm{in}}$ is about 0.05 eV larger with both B86r and D3 than the ideal value of formation energy per atom when Cu (111) is entirely covered by hBN. This is thought to be related also to the curl of hBN island, and we discuss this point in subsection 3.6.

Figure 6 shows the fluctuations of ε_{B}, ε_{N}, and $\varepsilon_{\mathrm{in}}$ calculated by utilizing 10 patterns of system of equations. In comparison to the fluctuations of ε_{B} and ε_{N}, $\varepsilon_{\mathrm{in}}$ exhibits the most significant variation, which is thought to result from the fluctuation of $\varepsilon_{\mathrm{in}}$ on the hBN islands with 6 six-membered rings. The fluctuation of $\varepsilon_{\mathrm{in}}$ comes from that of the curl of hBN islands.

We calculated the formation energies of the most stable structures for each n_{B} (n_{N}) using Eq. (6), along with the average values of ε_{B}, ε_{N}, and $\varepsilon_{\mathrm{in}}$. Subsequently, we compared them with the line connecting the most stable points (min. line), confirming their rough agreement with the raw data (Fig. 5). Thus, we are able to prove that our approximate approach with Eq. (6) is reasonably reliable.

3.5 Evaluation of critical size for the hBN island growth

In considering crystal growth, investigating the size at which an island initiates spontaneous growth is a crucial factor of the discussion. This size, known as the critical size, is a significant physical parameter for predicting the growth mechanism.

Our first-principles calculations focused on hBN islands with 1-10 six-membered rings. Naturally, experimentally observed islands are much larger than those studied in our calculations.[10-22] Critical sizes should be also typically quite larger than what can be calculated through the first-principles calculations. Consequently, obtaining the critical size

directly from the first-principles calculations is hopelessly impossible due to computational resource limitations.

Then, we have developed a method to predict the critical size by numerically extrapolating the shape and stability of larger islands in a semi-empirical manner based on the results obtained from calculations of islands with 1-10 six-membered rings. Assuming a simple and elemental theory, we conducted the following analysis.

Using ε_{B}, ε_{N}, and $\varepsilon_{\mathrm{in}}$, we investigated the size of hBN islands at which the inside atoms effect surpasses the edge effect, leading to negative formation energy. The considered shapes for hBN islands were restricted to triangles with B edge or with N edge. This is imposed as distinguishing hBN islands with armchair edge or those with an equal number of edge B and edge N is not feasible. Therefore, we have no choice but to disregard shapes other than triangles. The formation energies of Btri and Ntri can be calculated by

$$E_{\mathrm{f}} = 3n_{\mathrm{br}}\varepsilon_{\mathrm{B}} + 3\varepsilon_{\mathrm{N}} + (2n_{\mathrm{tr}} - 2)\varepsilon_{\mathrm{in}}, \quad (8)$$

$$E_{\mathrm{f}} = 3n_{\mathrm{br}}\varepsilon_{\mathrm{N}} + 3\varepsilon_{\mathrm{B}} + (2n_{\mathrm{tr}} - 2)\varepsilon_{\mathrm{in}}, \quad (9)$$

respectively, where n_{br} is the number of six-membered rings corresponding to the base of the triangle, and n_{tr} the total number of six-membered rings in the hBN island. Additionally, the relationship $n_{\mathrm{tr}} = \frac{1}{2}\, n_{\mathrm{br}}\,(n_{\mathrm{br}} + 1)$ holds between n_{br} and n_{tr}. We calculated the threshold value of n_{br} for which E_{f} becomes negative value from positive by Eqs. (8) and (9). The negative E_{f} means that the inside atoms effect surpasses the edge effect. Subsequently, using the ideal B-B and N-N distance of 2.556 Å in our hBN island geometry, we calculated the lateral size length (l), given by $l = 2.556 \times n_{\mathrm{br}}$. Then, using the threshold of n_{br}, we calculated the minimum lateral size length (l_{min}). Moreover, we calculated the critical size length (l_{c}), at which E_{f} is maximum, based on the same equation.

First, we calculated triangular islands with B edge using Eq. (8). In the B-rich case, n_{br}, n_{tr}, l_{min}, and l_{c} are 154, 11935, 39 nm, and 20 nm, respectively, with B86r, and 63, 2016, 16 nm, and 8 nm, respectively, with D3. On the other hand, in the N-rich case, they are 573, 164451, 146 nm, and 73 nm, respectively, with B86r, and 94, 4465, 24 nm, and 13 nm, respectively, with D3. Since ε_{B} is more stable in the B-rich, l_{min} becomes smaller than in the N-rich. Furthermore, the choice of B86r or D3 significantly affects the value of l_{min}. In the B-rich case, the difference of $\varepsilon_{\mathrm{in}}$ between B86r and D3 is 0.03 eV, so the value of l_{min} differs by about twice, and in the N-rich, it is 0.05 eV, so the difference is six times larger. Care must be taken regarding this, as the calculated values differ greatly between B86r and D3.

Next, we calculated triangular islands with N edge using Eq. (9). In the B-rich case, n_{br},

n_{tr}, l_{min}, and l_{c} are 212, 22578, 54 nm, and 27 nm, respectively, with B86r, and 80, 3240, 20 nm, and 10 nm, respectively, with D3. On the other hand, in the N-rich case, they are 159, 12720, 41 nm, and 20 nm, respectively, with B86r, and 27, 378, 7 nm, and 3 nm, respectively, with D3. Since ε_{N} is more stable in the N-rich, l_{min} becomes smaller than in the B-rich. Also, as in the case of triangular islands with B edge, l_{min} differs greatly due to the difference in $\varepsilon_{\mathrm{in}}$ between B86r and D3.

Figures 7 (a) and (b) show the formation energies calculated using equations (8) and (9) as the function of l for the aforementioned results for B86r and D3, respectively. We compared the cases of triangular islands with B edge and with N edge based on the size of l_{c}. The value of l_{c} is half of l_{min}, and in the B-rich case, the size of l_{c} is smaller in triangular islands with B edge than with B86r by 7 nm and with D3 by 2 nm. On the other hand, in the N-rich case, l_{c} is smaller in triangular islands with N edge than with B86r by 53 nm and with D3 by 10 nm. Therefore, comparing the cases of triangular islands with B edge and with N edge, l_{c} of triangular islands with N edge is smaller over wide range of $\bar{\mu}_{\mathrm{N}}$. The smaller l_{c} indicates that the island is more likely to spontaneously grow larger. This result indicates that islands are easier to grow into triangular islands with N edge than into those with B edge.

However, if we were to extend this method directly to the non-triangular case, the non-triangular structure would not be stable, even though the size becomes macroscopic. This is inconsistent with our calculation results for 6 and 10 six-membered rings. Additionally, it cannot be compared with the previous theoretical report for macroscopic islands.[23] Therefore, more advanced analysis method is strongly required, but it remains for the future work.

3.6 Curl of hBN island

In this subsection, we examined the curl effect of hBN islands. First, for the hBN island, we defined *d* as the difference in height between the farthest atom and the nearest atom from the Cu surface (Fig. 8). Then, we evaluated this *d* as the measure of curl and compared the cases of hBN islands with 10 six-membered rings. The curl of the labeled structures Btri, Ntri, BNrib, and BNa are shown in Fig. 8 (a)-(d), while unlabeled structures ex1–ex8 are shown in Fig. S12. Upon comparing the size of *d*, it is remarkable that d = 0.441 Å in Ntri, which is smaller than in other structures. This trend of Ntri exhibiting a smaller curl was consistently observed for hBN islands with 3 and 6 six-membered rings (Figs. S13 and S14). Additionally, as the island expand, the curl magnifies while maintaining the chemical bond

between the edge atoms and Cu atoms. Therefore, except for Ntri, hBN islands are thought to curl into a dome shape as their size becomes larger.

The observed curl is thought to be associated with the fact that $\varepsilon_{\mathrm{in}}$, as derived in subsection 3.4 is 0.05 eV larger than the formation energy per atom of the system in which Cu(111) is entirely covered by hBN. Since the hBN that covering the entire Cu(111) is ideally flat, the inside atoms effect differs from that of the curled hBN island. Furthermore, the distance between hBN covering the entire Cu(111) and the Cu surface is 2.907 Å with B86r and 3.008 Å with D3. This is larger by 0.718 Å with B86r and 0.827 Å with D3 compared to the distance between the inside atoms of Ntri, which has 3 six-membered rings, and the Cu surface. Therefore, it is inferred that the difference in the distance between the hBN islands and the Cu surface is also related to the difference in the effect of $\varepsilon_{\mathrm{in}}$.

The fluctuation of $\varepsilon_{\mathrm{in}}$ is larger than that of ε_{B} and ε_{N}, yet no significant correlation with *d* was observed. Instead, the substantial fluctuation of $\varepsilon_{\mathrm{in}}$ is thought to be associated with the distance between the hBN island and the Cu surface, *dd*. In the hBN island with 6 six-membered rings, ex4, for which the maximum value of $\varepsilon_{\mathrm{in}}$ was calculated, *dd* was 2.224 Å with B86r and 2.350 Å with D3. Conversely, in the hBN island with 6 six-membered rings, ex2, for which the minimum value of $\varepsilon_{\mathrm{in}}$ was calculated, *dd* was 2.368 Å with B86r and 2.455 Å with D3. In other structures, *dd* falls within this range. Therefore, as *dd* increases, $\varepsilon_{\mathrm{in}}$ monotonically decreases, suggesting its involvement in the fluctuation of $\varepsilon_{\mathrm{in}}$.

The discrepancy between the calculated value of $\varepsilon_{\mathrm{in}}$ and the ideal $\varepsilon_{\mathrm{in}}$ can be attributed to the relatively small size of the hBN island we calculated. Here, the ideal value of $\varepsilon_{\mathrm{in}}$ is −0.06 eV with B86r and −0.11 eV with D3, and the ideal distance is 2.907 Å with B86r and 3.008 Å with D3. As the size of the hBN island expands, the edge effect diminishes, *dd* approaches the ideal value, and $\varepsilon_{\mathrm{in}}$ should also tend towards the ideal value. When $\varepsilon_{\mathrm{in}}$ approaches the ideal value, l_{c} of triangular islands with B edge is 7 nm with B86r and 4 nm with D3 in the B-rich, and 12 nm with B86r and 7 nm with D3 in the N-rich. On the other hand, l_{c} of triangular islands with N edge is 9 nm with B86r and 4 nm with D3 in the B-rich, and 3 nm with B86r and 2 nm with D3 in the N-rich. These values are considerably smaller than those obtained using our calculated $\varepsilon_{\mathrm{in}}$. These mean that smaller islands can spontaneously grow up larger, when $\varepsilon_{\mathrm{in}}$ approaches the ideal value. Additionally, the discrepancy between our calculated $\varepsilon_{\mathrm{in}}$ and the ideal value can be attributed to be edge effect.

3.7 Discussion

We have conducted the aforementioned theoretical studies and now proceed to compare them with experimental observations. It is important to note that, in contrast to our calculated geometry, the islands observed in experiments exhibit much huge in sizes. Our calculations for small hBN islands consistently indicate that, in all cases, the most stable chemical potential range is wider for Ntri than for Btri. This observation suggests that the triangular islands observed in the CVD growth experiments have N edge.[13-15, 18, 20-22)] To predict the stability of triangular islands with B edge and with N edge for large hBN islands, where the assumption is that only triangular islands can be formed, using Eqs. (8) and (9). Triangular islands with B edge are stable when $\bar{\mu}_{\mathrm{N}}$ is in the range of 0 to 0.22 with B86r and 0 to 0.16 with D3. In contrast, triangular islands with N edge are stable when in the range of 0.22 to 1.0 with B86r and 0.16 to 1.0 with D3. Therefore, triangular islands with N edge are more stable over a wider chemical potential range.

Furthermore, with an increase in the number of six-membered rings to 3, 6, and 10, the range of the most stable $\bar{\mu}_{\mathrm{N}}$ for non-triangular hBN islands expand. Therefore, as the size of the islands become larger, the formation of triangular islands can be anticipated only in very specific conditions, either B-rich or N-rich. However, it is noteworthy that the majority of hBN islands, as observed in experiments utilizing Cu substrates, predominantly grow in triangular shapes.[13, 15, 18, 20, 21)]

Summarizing the preceding discussion, our results lead us to predict that the experimental conditions are relatively close to the N-rich condition. However, in actual CVD growth experiments of hBN, $B_3N_3H_6$ and BH_3-NH_3 are utilized as source materials. Given that $\bar{\mu}_{\mathrm{N}}$ should be around 0.5, a straightforward consideration appears inconsistent with our speculation. We think that part of the reason for this inconsistency may be attributed to the stability of monomer B and N. According to the results of our own calculations, monomer B is the most stable on the Cu subsurface, while monomer N is the most stable on the outermost surface. This suggests that, during CVD growth, B dissolves within the Cu substrate, leading to N-rich condition on Cu surface. The absence of H consideration in our calculations might also contribute to this deviation. In this study, we focused on bare edges, excluding factors such as H termination. We anticipate that incorporating H into our calculation will enable us to elucidate its role in CVD growth, providing comprehensive data and discussion to support experimental findings. detailed data and discussion to support the experimental facts. Additionally, the observed differences in curl sizes of Btri and Ntri in our calculations suggest that the curl effect may play some significant role. Investigating the relationship between curl and stability in hBN islands serves as motivation for future research.

We are now ready to discuss much deeper about our results. We have identified two noteworthy aspects: firstly, in the case of small islands, there is no chemical potential range where the armchair edge becomes stable; secondly, the bonds between edge N and Cu are strong, while those between edge B and Cu are comparatively weaker.

As the hBN island expands, our calculations reveal that the chemical potential range where non-triangles are most stable becomes wider, particularly near $\bar{\mu}_{\mathrm{N}} = 0.5$. However, for small islands, as per our calculated geometry, structures with exclusively armchair edges are not stable. Instead, structures with approximately equal lengths of B and N edges, such as BNmix and BNrib, exhibit as the most stable. This characteristic has not been reported in previous theoretical studies.

Considering that the size of our island, calculated using the first-principles calculations, is exceedingly small, our data alone are insufficient for a detailed discussion of this factor. While Eq. (6) and Fig. 6 address edges stability and inside atoms stability, we have not been able to make a distinction between armchair edge and zigzag edge. We delve into this aspect using the results reported by Zhang, et al., which assumes extremely large island size.[23)]

Zhang, et al. leverage the periodicity of the unit cell to perform calculations, assuming macro-sized hBN islands. Based on their calculations, they assert that for sufficiently large islands, armchair edge is more stable than either B edge or N edge. Here, the B edge is zigzag edge terminated with B, and the N edge is zigzag edge terminated with N, consistent with the definition in our study. Contrastingly, the non-triangular structure that proves most stable in our calculations is BNmix and BNrib. BNmix has both armchair and zigzag edges, and BNrib has B edge and N edge with nearly same length. From these findings, as the island grows larger, the structure with nearly identical length of B edge and N edge might become more stable than the structure with only armchair edge. The structure with a balanced number of B and N on the edge might tend to achieve stability.

We propose that the reason may be associated with the dangling bonds present at the edges and their bonding and ionic properties. Structurally, hBN islands feature dangling bonds at their edges, contributing significantly to their stability in relation to bonding with Cu. Therefore, the edge exerts a dominant effect, while the inside atoms have a comparatively weak effect. Moreover, it is noteworthy that edge N exhibits greater stability than edge B. Additionally, the Cu bond with edge N is strong, whereas the Cu bond with edge B is comparatively weaker. As a result, our findings indicate that edge N is more stable than edge B. Specifically, in our calculations, in the B-rich, ε_{B} is 0.39 eV more stable than ε_{N}.

Conversely, in the N-rich, ε_{B} is 1.39 eV less stable than ε_{N}. These are the results of B86r calculation. On average, ε_{B} is approximately 0.5 eV less stable than ε_{N}.

The edges of the hBN islands form strong bonds with the substrate Cu, while the inside atoms only bond van der Waals forces with Cu, which are neither ionic nor covalent. Naturally, the van der Waals force bonds are considerably weaker than other chemical bonds, emphasizing the dominance of the edge effect. Additionally, owing to ionization tendencies, B and Cu exhibit a tendency to become positive ions, while N tends to become a negative ion. Consequently, for both edge B and edge N, the latter experiences stronger ionic bonding with Cu. Therefore, edge N is considered more stable than edge B.

However, for a more detailed examination, it is insufficient to solely concentrate on the disparity between B edge and N edge. We also need to meticulously assess the differences in stability between structures with solely armchair edge and those featuring B edge and N edge of equal length, particularly when the island reaches a sufficiently large size. We acknowledge that these are matters to be addressed in future work.

Finally, we discuss the distinctions between B86r and D3. Substantial variations exist in $\varepsilon_{\mathrm{in}}$ and the distance between the hBN islands and the Cu surface. With D3, $\varepsilon_{\mathrm{in}}$ is 0.3 to 0.4 eV lower than compared to B86r, while the *dd* is 0.87 to 1.3 Å longer. However, there is no noteworthy difference in the most stable structure of hBN islands. Generally, B86r demonstrates higher accuracy and reliability, albeit at a higher computational cost.[27, 31)]

4. Conclusions

We directed our attention to the shape of small monolayer hBN islands on Cu(111), assuming intrinsic nucleation during the initial CVD growth utilized the first-principles calculations based on the DFT. First, we found that desorption is not a determining factor in island shape of growing hBN islands during the CVD growth. As the hBN island expands, the chemical potential range in which the non-triangular shapes become most stable widens, particularly around $\bar{\mu}_{\mathrm{N}} = 0.5$. However, for small islands, such as in our calculated geometry, there is no chemical potential range where the armchair edge becomes stable. Using Eq. (6), we clarified the difference between the effects of edge and inside atoms, and revealed that the edge effect is dominant. This is attributed to the fact that the edges feature dangling bonds, leading to ionic and covalent interactions with the Cu atoms on the surface, whereas the non-edge parts lack dangling bonds and consequently exhibit only weak van der Waals interactions. Additionally, the bond between edge N and Cu is strong, while the bond

between edge B and Cu is comparatively weaker. This discrepancy arises from the tendency of B and Cu to form positive ions, and N to form negative ions, influenced by their ionization tendencies. Therefore, edge N is more stable than edge B, given its stronger ionic bonding with Cu. We additionally proposed that triangular hBN islands exhibit an N edge due to the greater stability of ε_{N} compared to ε_{B}. Furthermore, our results indicated that triangular islands with N edge tend to grow more spontaneously than triangular islands with B edge because the l_{c} is smaller for triangular islands with N edge over a substantial range of $\bar{\mu}_{\mathrm{N}}$. This led us to infer a connection between the curl effect and N edge hBN islands. In fact, the curl effect enhances our $\varepsilon_{\mathrm{in}}$ compared to the ideal value.

Acknowledgments

This study is partially supported by KAKENHI (21H01768, 21H01394). This research used the supercomputer of ISSP, Univ. of Tokyo, and the supercomputer FUGAKU of Riken. Atomic models are depicted with VESTA.[36)]

References

1) K. Watanabe, T. Taniguchi, and H. Kanda, Nature Mater. **3**, 404 (2004).
2) T. Taniguchi and K. Watanabe, J. Cryst. Growth **303**, 525 (2007).
3) C. R. Dean, A. F. Young, I. Meric, C. Lee, L. Wang, S. Sorgenfrei, K. Watanabe, T. Taniguchi, P. Kim, K. L. Shepard, and J. Hone, Nature Nanotech. **5**, 722 (2010).
4) N. Fang, S. Toyoda, T. Taniguchi, K. Watanabe, and K. Nagashio, Adv. Funct. Mater. **29**, 1904465 (2019).
5) T. Uwanno, T. Taniguchi, K. Watanabe, and K. Nagashio, ACS Appl. Interfaces **10**, 28780 (2018).
6) X. Cui, G. H. Lee, Y. D. Kim, G. Arefe, P. Y. Huang, C. H. Lee, D. A. Chenet, X. Zhang, L. Wang, F. Ye, F. Pizzocchero, B. S. Jessen, K. Watanabe, T. Taniguchi, D. A. Muller, T. Low, P. Kim, and J. Hone, Nature Nanotech. **10**, 534 (2015).
7) J. Xue, J, Sanchez-Yamagishi, D, Bulmash, P, Jacquod, A, Deshpande, K. Watanabe, T. Taniguchi, P. Jarillo-Herrero, and B. J. LeRoy, Nature Mater. **10**, 282 (2011).
8) K. Takeyama, R. Moriya, K. Watanabe, S. Masubuchi, T. Taniguchi, and T. Machida, Appl. Phys. Lett. **117**, 153101 (2020).
9) K. Kinoshita, R. Moriya, S. Okazaki, Y. Zhang, S. Masubuchi, K. Watanabe, T. Taniguchi, T. Sasagawa, and T. Machida, Nano Lett. **22**, 4640 (2022).
10) S. Fukamachi, P. Solis-Fernandez, K. Kawahara, D. Tanaka, T. Otake, Y. C. Lin, K. Suenaga, and H. Ago, Nature Electron. **6**, 126 (2023).
11) Y. Uchida, S. Nakandakari, K. Kawahara, S. Yamasaki, M. Mitsuhara, and H. Ago, ACS Nano **12**, 6236 (2018).
12) Y. Uchida, K. Kawahara, S. Fukamachi, and H. Ago, ACS Appl. Electron. Mater. **2**, 3270 (2020).
13) K. K. Kim, A. Hsu, X. Jia, S. M. Kim, Y. Shi, M. Hofmann, D. Nezich, J. F. Rodriguez-Nieva, M. Dresselhaus, T. Palacios, and J. Kong, Nano Lett. **12**, 161 (2012).
14) C. M. Orofeo, S. Suzuki, H. Kageshima, and H. Hibino, Nano Research **6**, 335 (2013).
15) Y. Ji, B. Calderon, Y. Han, P. Cueva, N. R. Jungwirth, H. A. Alsalman, J. Hwang, G. D. Fuchs, D. A. Muller, and M. G. Spencer, ACS Nano **11**, 12057 (2017).
16) G. Kim, A. R. Jang, H. Y. Jeong, Z. Lee, D. J. Kang, and H. S. Shin, Nano Lett. **13**, 1834 (2013).
17) Y. Gao, W. Ren, T. Ma, Z. Liu, Y. Zhang, W. B. Liu, L. P. Ma, X. Ma, and H. M. Cheng, ACS Nano **7**, 5199 (2013).
18) X. Song, J. Gao, Y. Nie, T. Gao, J. Sun, D. Ma, Q. Li, Y. Chen, C. Jin, A. Bachmatiuk, M.

H. Rummeli, F. Ding, Y. Zhang, and Z. Liu, Nano Research **8**, 3164 (2015).

19) W. H. Lin, V. W. Brar, D. Jariwala, M. C. Sherrott, W. S. Tseng, C. I. Wu, N. C. Yeh, and H. A. Atwater, Chem. Mater. **29**, 4700 (2017).
20) L. Wang, X. Xu, L. Zhang, R. Qiao, M. Wu, Z. Wang, S. Zhang, J. Liang, Z. Zhang, Z. Zhang, W. Chen, X. Xie, J. Zong, Y. Shan, Y. Guo, M. Willinger, H. Wu, Q. Li, W. Wang, P. Gao, S. Wu, Y. Zhang, Y. Jiang, D. Yu, E. Wang, X. Bai, Z. J. Wang, F. Ding, and K. Liu, Nature **570**, 91 (2019).
21) T. A. Chen, C. P. Chuu, C. C. Tseng, C. K. Wen, H. -S. P. Wong, S. Pan, R. Li, T. A. Chao, W. C. Chueh, Y. Zhang, Q. Fu, B. I. Yakobson, W. H. Chang, and L. J. Li, Nature **579**, 219 (2020).
22) S. Wang, J. Crowther, H. Kageshima, H. Hibino, and Y. Taniyasu, ACS Nano **15**, 14384 (2021).
23) Z. Zhang, Y. Liu, Y. Yang, and B. I. Yakobson, Nano Lett. **16** 1398 (2016).
24) R. Imamura and H. Kageshima, extend abstract of 2023 International Workshop on Dielectric Thin Films for future electric devices -science and technology-, p. 49.
25) https://azuma.nims.go.jp.
26) P. E. Blochl, Phys. Rev. B **50**, 17953 (1994).
27) I. Hamada, Phys. Rev. B **91**, 119902 (2015).
28) S. Grimme, J. Antony, S. Ehrlich, and H. Krieg, J. Chem. Phys. **132**, 154104 (2010).
29) S. Ehrlich, J. Moellmann, W. Reckien, T. Bredow, and S. Grime, ChemPhysChem. **12**, 3414 (2011).
30) H. J. Monkhorst and J. D. Pack, Phys. Rev. B **13**, 5188 (1976).
31) F. Schulz, P. Liljeroth, and A. P. Seitsonen, Phys. Rev. Mater. **3**, 084001 (2019).
32) X. Gao, S. Wang, and S. Lin, ACS Appl. Mater. Interfaces **8**, 24238 (2016).
33) H. Zhu, J. Zhu, Z. Zhang, and R. Zhao, J. Phys. Chem. C **125**, 26542 (2021).
34) C. G. Van de Walle and J. Neugebauer, Phys. Rev. Lett. **88**, 066103 (2002).
35) Y. Liu, S. Bhowmick, and B. I. Yakobson, Nano Lett. **11**, 3113 (2011).
36) K. Momma and F. Izumi, J. Appl. Cryst. **44**, 1272 (2011).

Figure Captions

Figure 1. Top views of optimized structures of hBN islands on Cu(111), calculated with B86r. (a) Islands with 3 six-membered rings. (b) Islands with 6 six-membered rings. (c) Islands with 10 six-membered rings. (d) An example of grouping atoms in a hBN island (Ntri) into three: edge B, edge N, and inside atoms. Blue, green, and silver balls represent Cu, B, and N atoms, respectively.

Figure 2. Formation energies for each hBN islands on Cu(111) as the function of normalized chemical potential ($\bar{\mu}_{\mathrm{N}}$). (a) Islands with 3 six-membered rings. (b) Islands with 6 six-membered rings. (c) Islands with 10 six-membered rings. $\bar{\mu}_{\mathrm{N}} = 0$ and $\bar{\mu}_{\mathrm{N}} = 1$ correspond to B-rich and N-rich, respectively. The figures on the left and right represent the results calculated with B86r and with D3, respectively.

Figure 3. Chemical potential dependence of the most stable structure in hBN islands with 3, 6, and 10 six-membered rings on Cu(111). The filled and shaded zones represent the results calculated with B86r and D3, respectively.

Figure 4. The calculation results for free-standing hBN. (a) Examples of initial structure and final optimized structure of free-standing hBN islands. (b) Chemical potential dependence of the most stable structure in free-standing hBN islands with 3, 6, and 10 six-membered rings. The filled and shaded zones represent the results calculated with B86r and D3, respectively. (c) The structure of hBN island ex3 with 10 six-membered rings just removed from the Cu substrate. Green and silver balls represent B and N atoms, respectively.

Figure 5. Formation energies per atom as the function of hBN island size (number of B, n_{B}, or number of N, n_{N}). (a) The B-rich case as the function of n_{B}. (b) The B-rich case as the function of n_{N}. (c) The N-rich case as the function of n_{B}. (d) The N-rich case as the function of n_{N}. Blue and green dots represent the calculated value with B86r and D3, respectively. Dotted lines represent the most stable structure for each n_{B} (n_{N}). Blue and green lines correspond to B86r and D3, respectively. Broken lines represent the most stable value for

each n_{B} (n_{N}) as reproduced by Eq. (6). Light blue and orange lines correspond to B86r and D3, respectively.

Figure 6. ε_{B}, ε_{N}, and $\varepsilon_{\mathrm{in}}$ evaluated using Eq. (6). Circles, triangles, and squares represent ε_{B}, ε_{N}, and $\varepsilon_{\mathrm{in}}$, respectively. Red and blue dots represent B-rich and N-rich, respectively. The filled and the shaded zones are evaluated with B86r and D3, respectively.

Figure 7. Formation energies calculated using Eqs. (8) and (9) as the function of the island size length l. (a) Results calculated used ε_{B}, ε_{N}, and $\varepsilon_{\mathrm{in}}$ with B86r. (b) Results calculated used ε_{B}, ε_{N}, and $\varepsilon_{\mathrm{in}}$ with D3. Orange and blue lines represent results for triangular islands with B edge (TB) and with N edge (TN), respectively. Solid lines correspond to B-rich, while dotted lines correspond to N-rich.

Figure 8. Side views of hBN islands with 10 six-membered rings calculated with B86r. (a) In the case of Btri. (b) In the case of Ntri. (c) In the case of BNrib. (d) In the case of BNa. The parameter *d* is defined as the difference in height between the farthest atom from and the closest atom to the Cu surface.

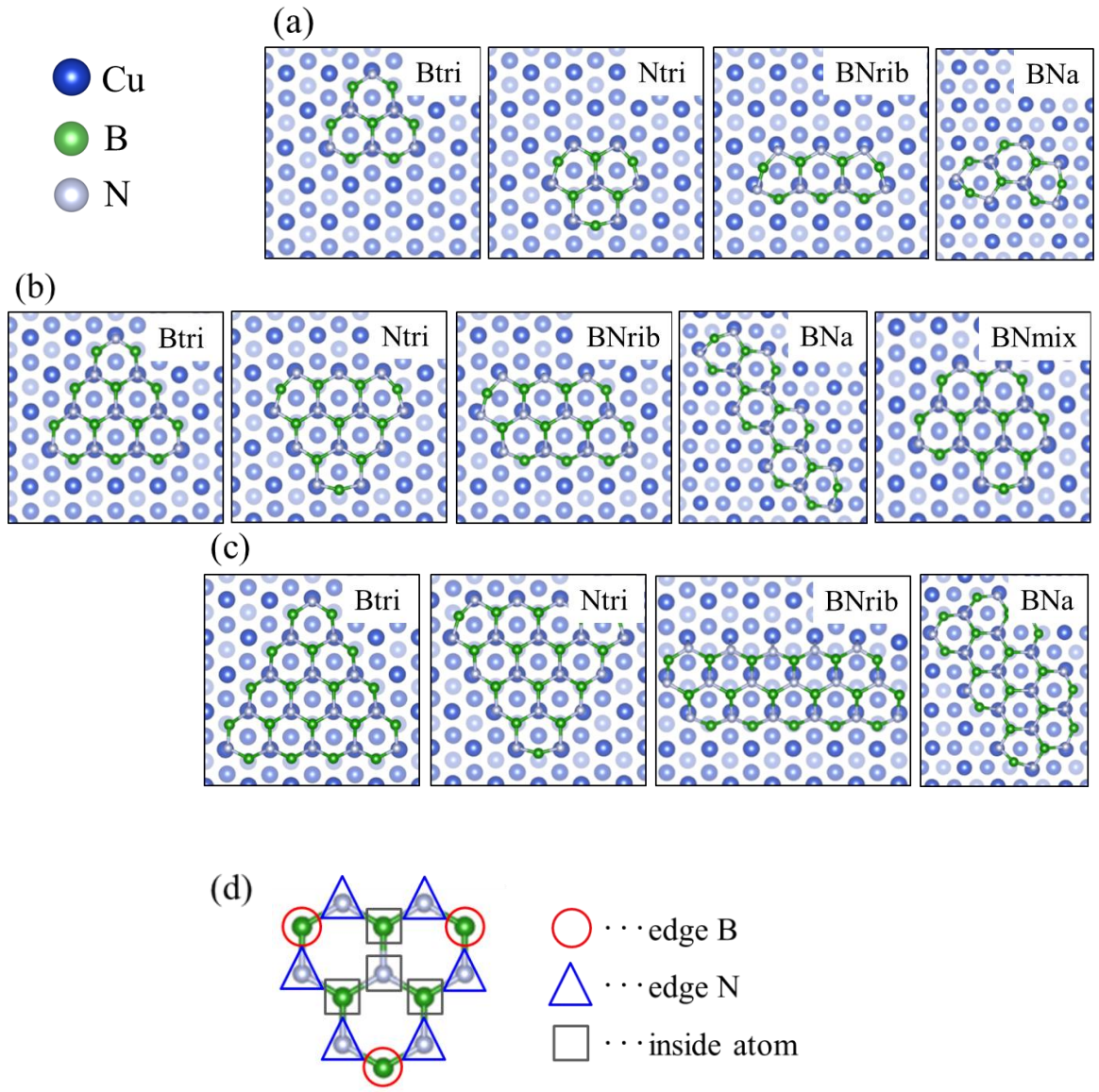
(a)
Cu
B
N
Btri
Ntri
BNrib
BNa
(b)
Btri
Ntri
BNrib
BNa
BNmix
(c)
Btri
Ntri
BNrib
BNa
(d)
· · · edge B
· · · edge N
· · · inside atom

Fig. 1.

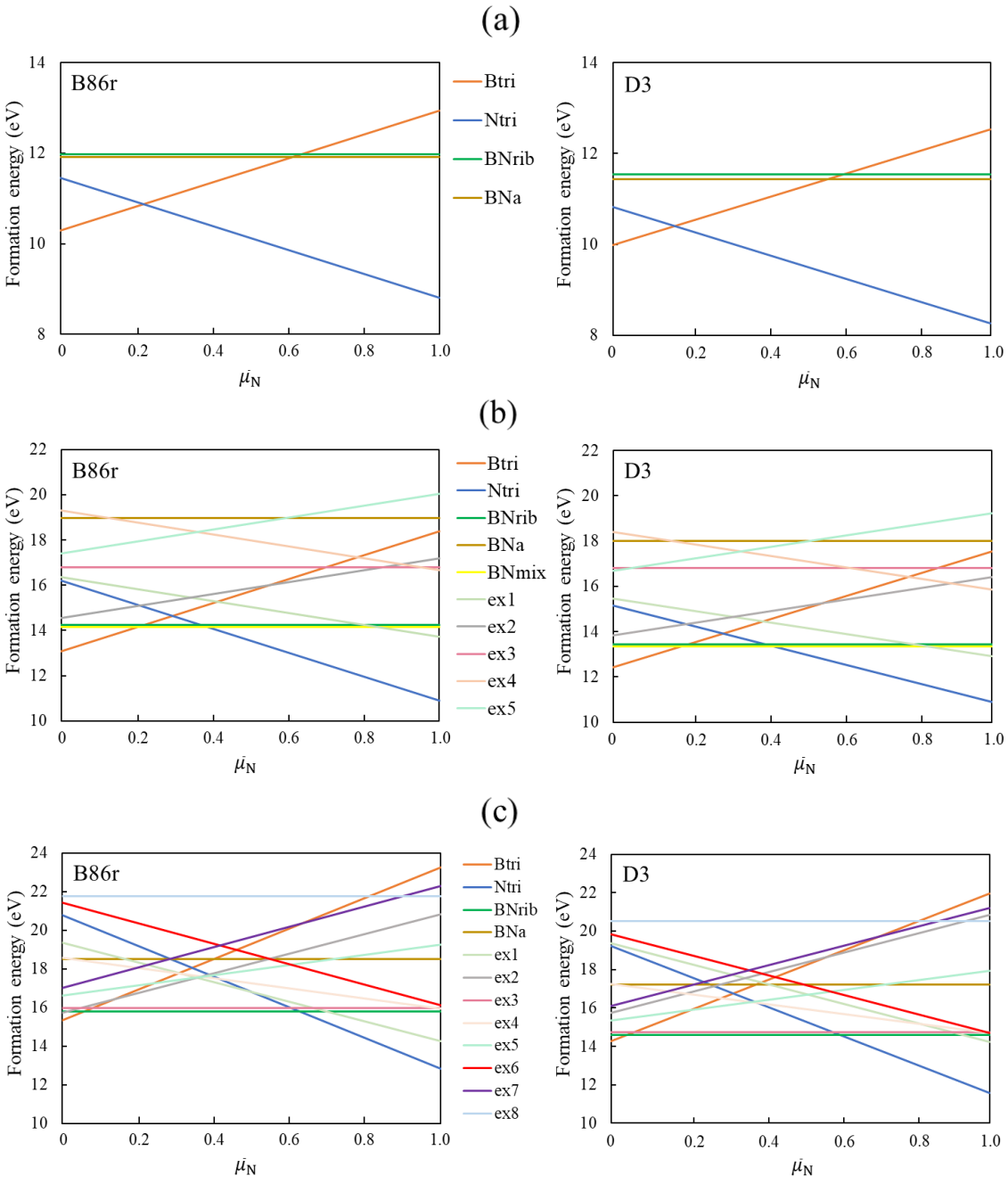
(a)
B86r
D3
Formation energy (eV)
μ_N
Btri
Ntri
BNrib
BNa
(b)
B86r
D3
Formation energy (eV)
μ_N
Btri
Ntri
BNrib
BNa
BNmix
ex1
ex2
ex3
ex4
ex5
(c)
B86r
D3
Formation energy (eV)
μ_N
Btri
Ntri
BNrib
BNa
ex1
ex2
ex3
ex4
ex5
ex6
ex7
ex8

Fig. 2.

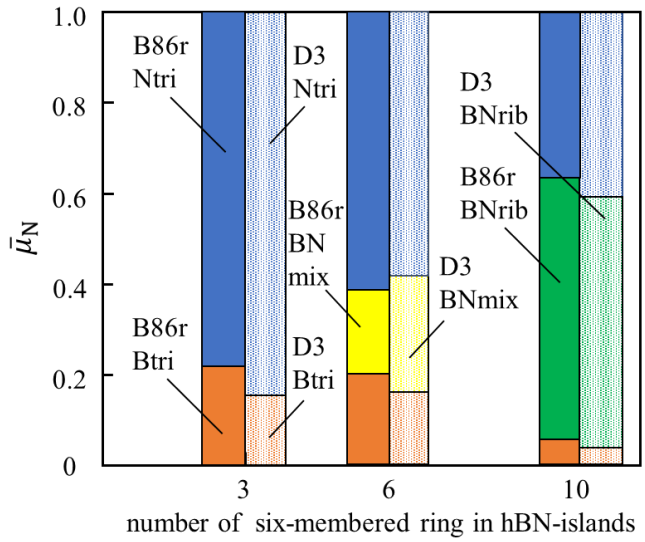
1.0
0.8
0.6
0.4
0.2
0
$\bar{\mu}_N$
B86r
Ntri
D3
Ntri
B86r
BN
mix
B86r
Btri
D3
Btri
D3
BNrib
B86r
BNrib
D3
BNmix
3
6
10
number of six-membered ring in hBN-islands

Fig. 3.

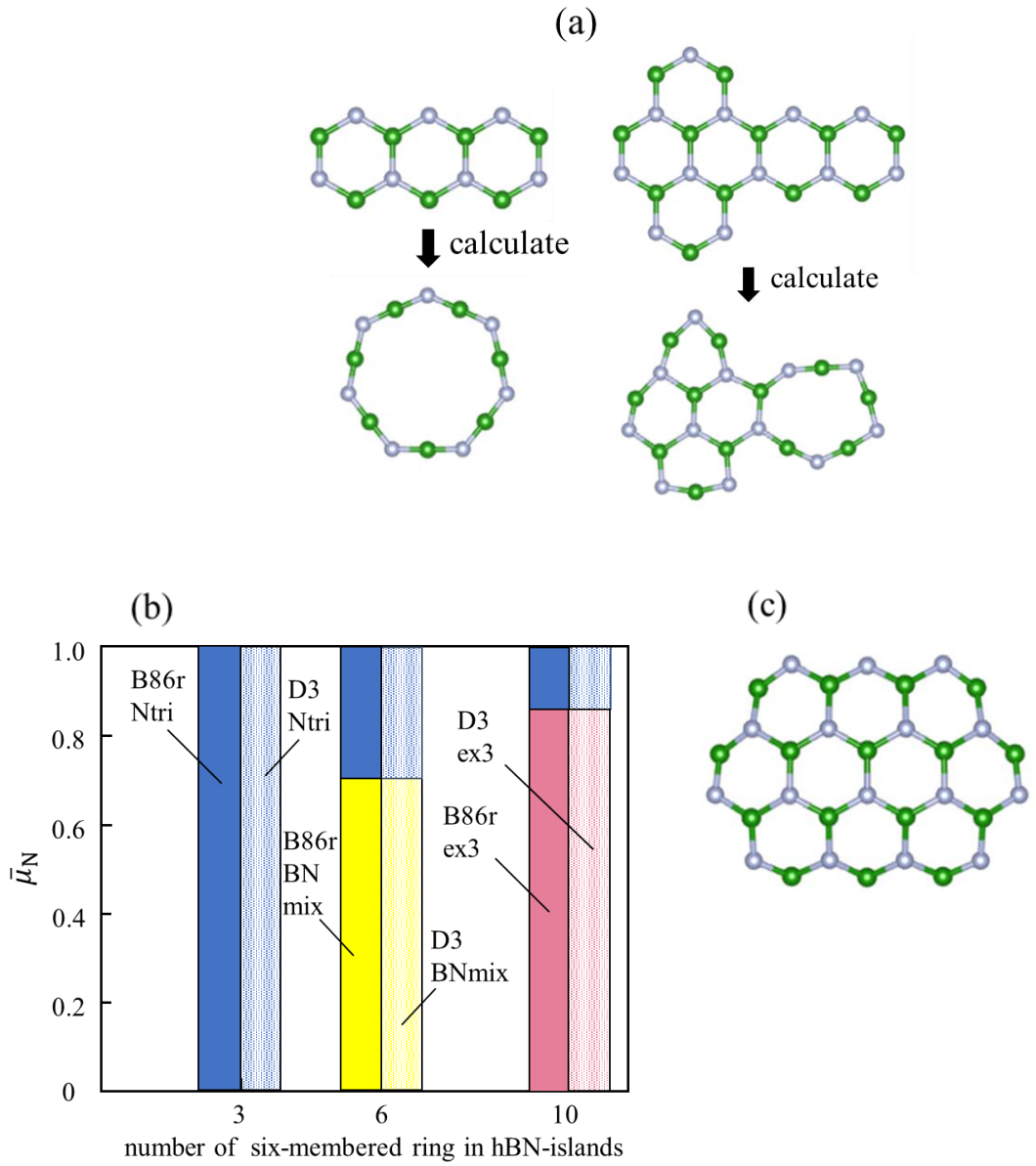
(a)
calculate
calculate
(b)
(c)
1.0
0.8
0.6
0.4
0.2
0
$\bar{\mu}_N$
B86r
Ntri
D3
Ntri
B86r
BN
mix
D3
BNmix
D3
ex3
B86r
ex3
3
6
10
number of six-membered ring in hBN-islands

Fig. 4.

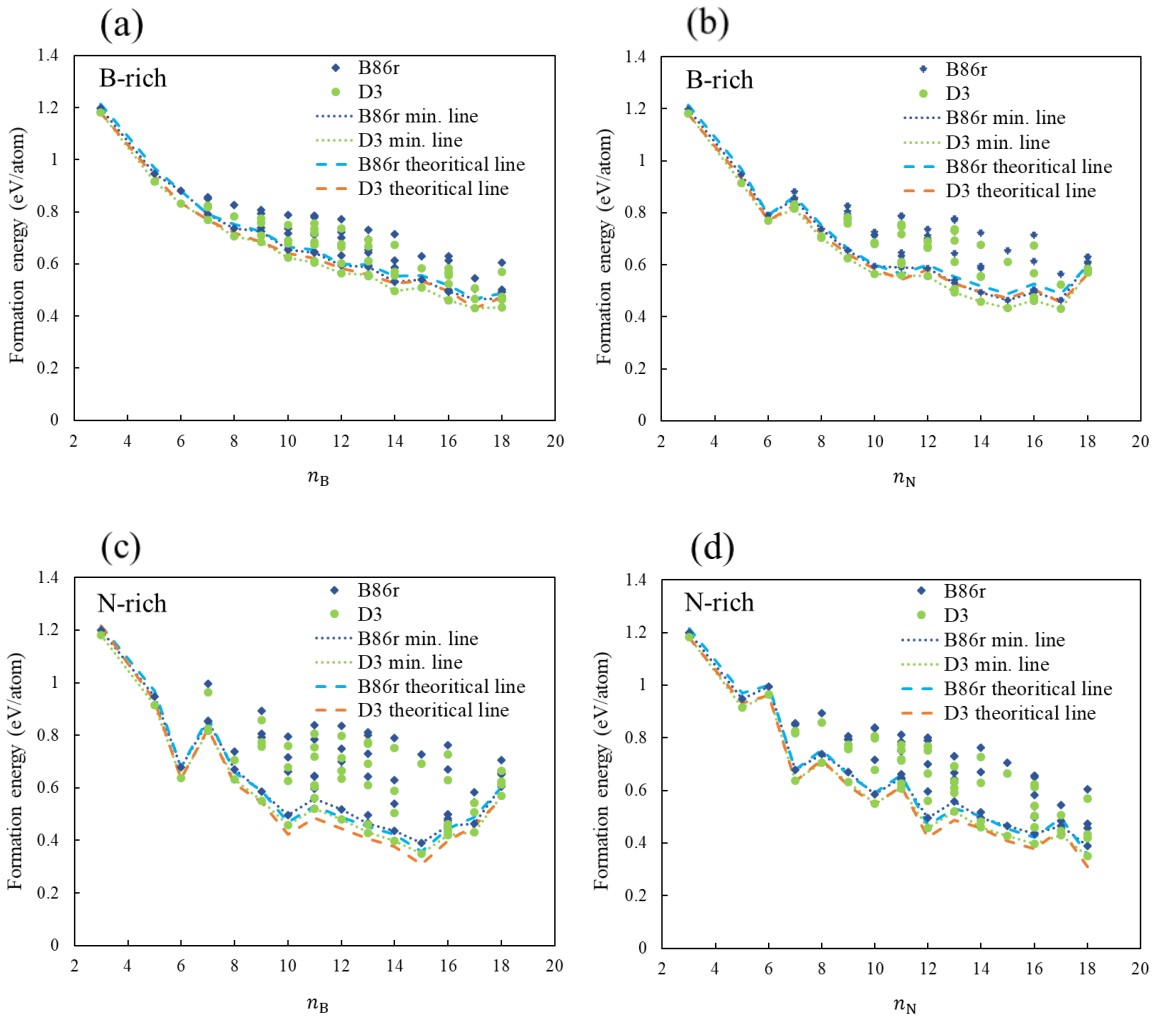
(a)
B-rich
B86r
D3
B86r min. line
D3 min. line
B86r theoritical line
D3 theoritical line
Formation energy (eV/atom)
n_B
(b)
B-rich
B86r
D3
B86r min. line
D3 min. line
B86r theoritical line
D3 theoritical line
Formation energy (eV/atom)
n_N
(c)
N-rich
B86r
D3
B86r min. line
D3 min. line
B86r theoritical line
D3 theoritical line
Formation energy (eV/atom)
n_B
(d)
N-rich
B86r
D3
B86r min. line
D3 min. line
B86r theoritical line
D3 theoritical line
Formation energy (eV/atom)
n_N

Fig. 5.

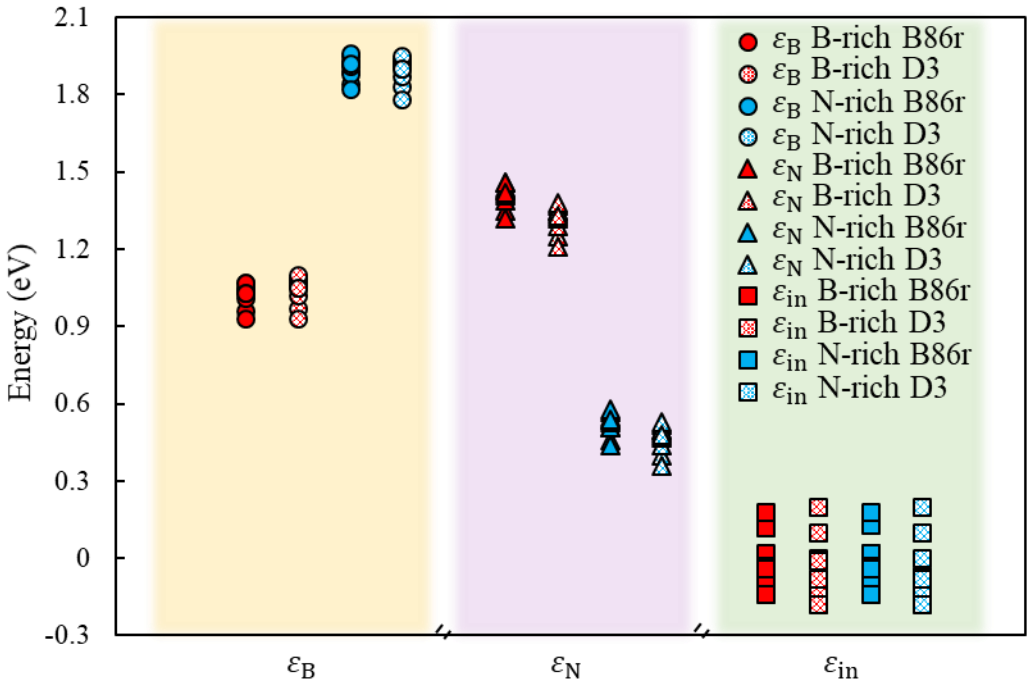
2.1
1.8
1.5
1.2
0.9
0.6
0.3
0
-0.3
Energy (eV)
ε_B B-rich B86r
ε_B B-rich D3
ε_B N-rich B86r
ε_B N-rich D3
ε_N B-rich B86r
ε_N B-rich D3
ε_N N-rich B86r
ε_N N-rich D3
ε_{in} B-rich B86r
ε_{in} B-rich D3
ε_{in} N-rich B86r
ε_{in} N-rich D3
ε_B
ε_N
ε_{in}

Fig. 6.

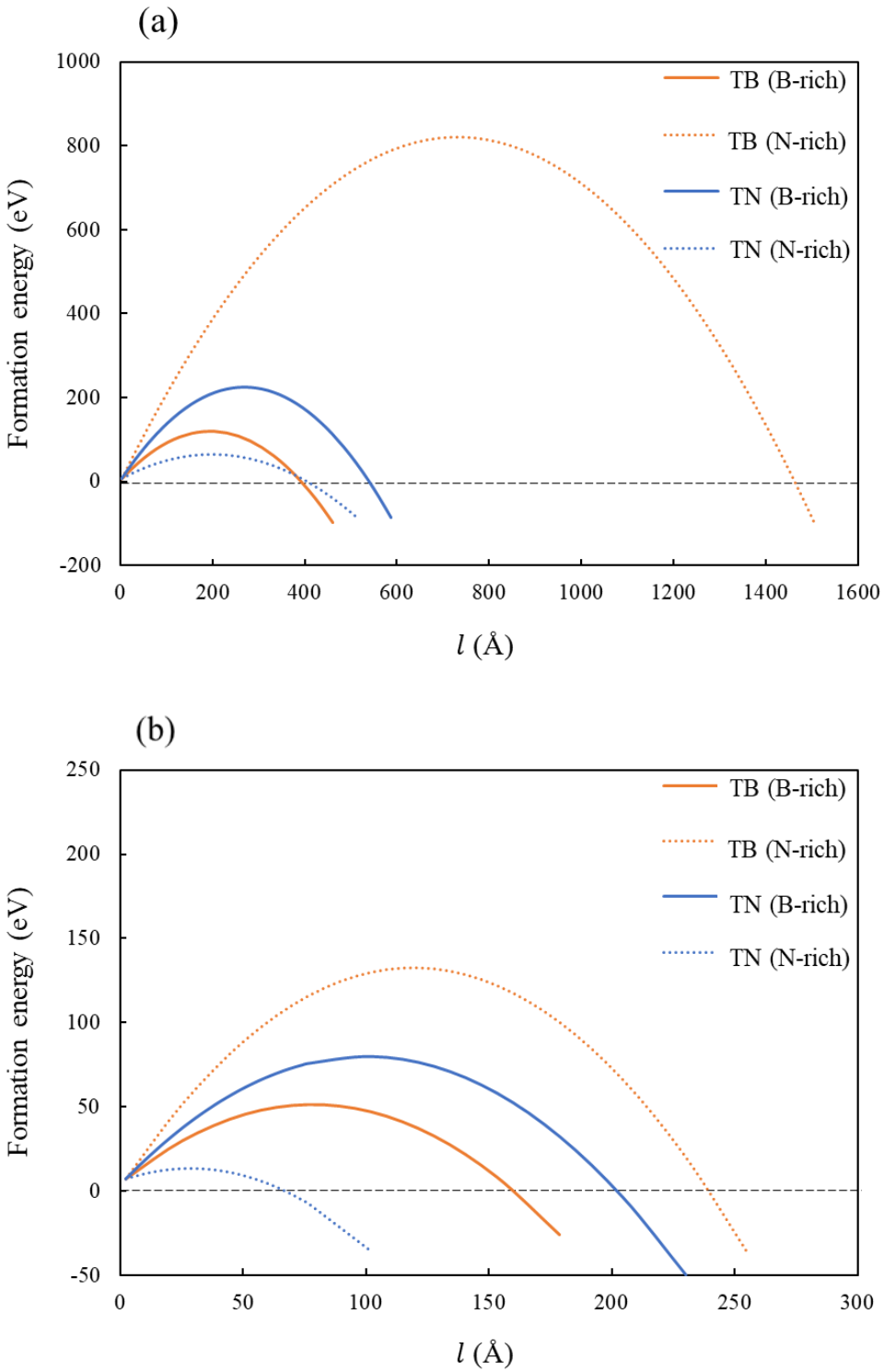
(a)
Formation energy (eV)
1000
800
600
400
200
0
-200
0
200
400
600
800
1000
1200
1400
1600
l (Å)
TB (B-rich)
TB (N-rich)
TN (B-rich)
TN (N-rich)
(b)
Formation energy (eV)
250
200
150
100
50
0
-50
0
50
100
150
200
250
300
l (Å)
TB (B-rich)
TB (N-rich)
TN (B-rich)
TN (N-rich)

Fig. 7.

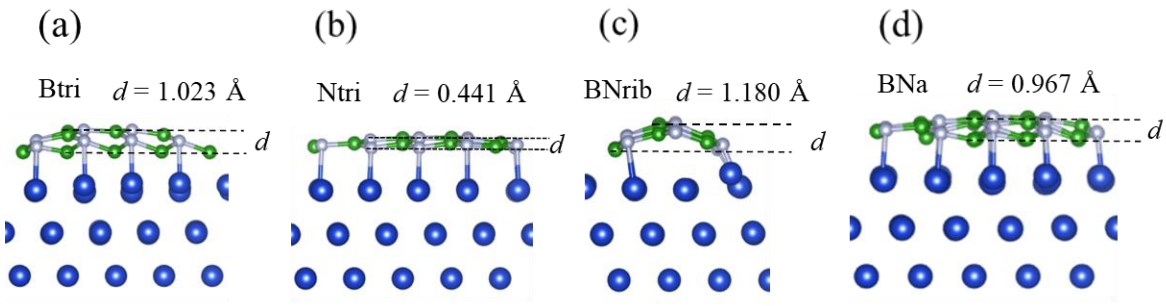

Fig. 8.